Journal of Sol-Gel Science and Technology (2022) 102:172–184
https://doi.org/10.1007/s10971-021-05579-x

ORIGINAL PAPER: CHARACTERIZATION METHODS OF SOL-GEL AND HYBRID MATERIALS

Controlling the local-ensemble structure in mesoporous hybrid titania-silica thin films containing aminopropyl groups

Alejandra Calvo[1,4] · Leandro Andrini[1] · Federico J. Williams[2] · José M. Ramallo-López[1] · Galo J. A. A. Soler-Illia[3] · Félix G. Requejo[1]

Received: 7 May 2021 / Accepted: 18 June 2021 / Published online: 19 August 2021

Abstract

Mesoporous hybrid materials containing inorganic and organic functional groups are relevant for advanced applications in separation, sorption or heterogeneous catalysis. The possibility of combining materials with high surface area and tailorable mesopore size with a mixed oxide framework and organic functions open the gate to imitating complex biosystems such as enzyme active sites. One of the critical aspects towards a multiscale control of these complex materials is the understanding of the actual framework structure and the interplay of the framework ions and the organic functions, and how these features are related to the sol-gel preparation conditions. In this work, mesoporous hybrid organic-inorganic thin films (MHTF) based on a mixed silica-titania matrix containing 20% aminopropyl functions were prepared and thoroughly studied by X-ray absorption spectroscopy at both the Ti and Si K-edges, and by O1s and N1s X-ray photoelectron spectroscopy. This approach permitted us to simultaneously probe the changes in Si and Ti coordination, the linkages between the inorganic centers, and the availability of the amino functions along samples with varying Si:Ti ratio. We find substantial differences between the local structure of pure inorganic oxides and the hybrid materials. In the oxides, increasing the %Ti leads to an increase in octahedral Si sites and Ti-oxo clusters with shorter Ti-O bonds. In the hybrid materials, higher Ti coordination with longer bonds are observed, along with a prevalence of Si centers with distorted tetrahedral coordination. These findings suggest that aminopropyl building blocks act as a compatibilizer between Ti(IV) and Si(IV) centers, leading to a hybrid mixed phase with large silica-titania interface. This intermixing also influences the exposition of amino groups at the pore surface. These aspects are of importance in the design of high surface area adsorbents, permselective membranes or heterogeneous catalysts.

Supplementary information The online version contains supplementary material available at https://doi.org/10.1007/s10971-021-05579-x.

✉ Galo J. A. A. Soler-Illia
gsoler-illia@unsam.edu.ar

✉ Félix G. Requejo
requejo@fisica.unlp.edu.ar

[1] Instituto de Investigaciones Fisicoquímicas Teóricas y Aplicadas (INIFTA) UNLP-CONICET, Diag. 113 y 64, 1900, La Plata, Argentina

[2] Departamento de Química Inorgánica, Analítica y Química Física, Facultad de Ciencias Exactas y Naturales, INQUIMAE-CONICET, Universidad de Buenos Aires, Buenos Aires C1428EHA, Argentina

[3] Instituto de Nanosistemas, Universidad Nacional de General San Martín, Av 25 de Mayo 1021, San Martín B1650KNA, Argentina

[4] Present address: YPF Tecnología S. A., Av. del Petróleo Argentino, Provincia de Buenos Aires, Berisso 900-1198, Argentina

Graphical Abstract

The structure of highly organized mesoporous thin films with aminopropyl groups and Si-Ti framework can be precisely determined by combining XANES and XPS. Functionality can be controlled from synthesis.

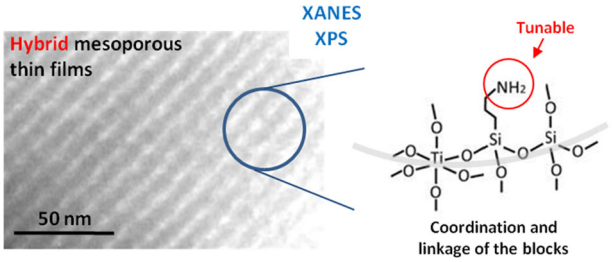

Keywords Mesoporous · Thin films · Mixed oxides · Hybrid materials · XANES

Highlights

- Highly organized mesoporous thin films with aminopropyl groups and Si-Ti framework are synthesized from a one-pot, low-temperature method.
- We present an exhaustive spectroscopic study of these materials by combining XANES and XPS.
- Ti and Si K-Edge XANES permit to assess the changes in bonding and coordination of both cations in mixed oxide and hybrid matrices.
- XPS measurements permit to understand the formation of Si-O-Ti interfaces and the availability of the amino groups.
- This study permits to link sol-gel processing conditions to the structure of complex hybrid mesoporous materials.

1 Introduction

The interest in hybrid organic-inorganic materials has leaped forward in the last two decades due to a wealth of potential applications [1–6]. The properties of hybrid materials are due to the synergy between the inorganic and organic components. An illustrative example is the metal oxide-based hybrid catalysts, where the surface sites of the inorganic scaffold play an important role as Brönsted acid centers, helping organic groups to accelerate the chemical reactions [7–10]. Thus, the inorganic scaffold is more than a mere support, in fact it cooperates synergistically with the catalytic process [11]. For example, Motokura et al. [12–14] have shown that certain features of this kind of hybrid materials are critical to the success of the catalysis, such as: (a) composition of the inorganic scaffold, (b) nature and distribution of the organic groups and (c) proximity and geometry between organic and inorganic centers.

Hybrid mesoporous materials present great interest due to their huge surface area and monodisperse pores, which offer prospective applications in catalysis, environment and biomaterials [15–18]. In particular, mesoporous hybrid thin films (MHTF) have been thoroughly investigated [19–21] aiming at a variety of applications such as selective sensors [22, 23], permselective membranes [24–28] and nanoreactors [29, 30]. However, due to the amorphous wall nature and the high dilution of species of interest in these materials, there is a limitation in the structural characterization at the local environment, which becomes crucial for the understanding of the origin of material properties and their consequent rational design. In particular, the controlled spatial assembly of catalytically active molecular species on the pore surface is essential, as cooperative activation effects between the dangling groups and the surface take place [31, 32], as have been observed in several silica-based mesoporous systems [33–38]. Thus, a thorough characterization of hybrid materials at the molecular and atomic level is crucial to determine the relationship between structure and properties for the controlled expanding of their scope to a wider range of applications.

An important limitation to characterize such sol–gel derived structures is the general absence of long- or medium-range order in the frameworks. Usually, hybrid materials are amorphous or present cluster-like domains that cannot be properly assessed by the usual X-Ray Diffraction techniques. Hence, spectroscopic methods providing both short range structure and chemical characterization are needed to understand the composition and the geometry of organic and inorganic building blocks. In this regard, X-ray Absorption Near Edge Structure (XANES) is a powerful technique to determine local atomic environments in materials of different nature [39, 40]. This technique is well-suited for mixed oxides, as the pre-edge peaks in K-edge XANES spectra of 3d

transition metals depend on the coordination number and symmetry of the surrounding atoms, providing a direct probe for the study of coordination [41] and symmetry [42]. Thus, XANES provides a molecular picture of the local structure around the absorbing atom in the hybrid materials studied here. Interestingly, XANES is suited to analyze mesoporous thin films, overcoming the limitations imposed by the extremely low sample mass, the presence of substrates, impurities, etc. In the past, we used this technique to determine the role of the local coordination of Ti(IV) sites in the photocatalytic performance of mesoporous titania thin films [43]. XANES has also proven to be an essential structural tool to characterize $Zr_{1-x}Si_xO_2$ mixed oxide mesoporous thin films with high cation interdispersion, permitting to assess the changes in site symmetry of Si(IV) and Zr(IV) along all the composition range [44]. Moreover, in the case of titania-silica mesoporous thin films, XANES permits to evaluate coordination changes in Ti(IV) sites which play a crucial roles in the optical, electronic and catalytic properties of the material [45]. This technique can be advantageously combined with X-Ray photoelectron spectroscopy (XPS), which gives a precise and quantitative measurement of chemical speciation at the material surface. In the case of MHTF, we have shown that XPS is a valuable tool to obtain complete structural information of the whole films [46].

In this work, we present an exhaustive spectroscopic study of mesoporous hybrid thin films made up of a mixed Ti/Si oxide framework that contains aminopropyl functions $(Si_{0.8-x}Ti_x(Si(CH_2CH_2CH_2NH_2))_{0.2}O_{1.9}$, by combining XANES and XPS. We take advantage of the chemical selectivity of XANES performing systematic experiments at the Ti and Si K-edge in samples with a variable Si:Ti ratio. In addition, we carried out XPS measurements in order to gain insight into the surface chemical composition including the connectivity between the inorganic centers and the availability of the amino function. We thus provide a thorough spectroscopic characterization of a complex system such as mesoporous hybrid organic–inorganic thin films based on a mixed oxide framework composed of two cations with different chemistry, that can be intimately intermixed and integrated with an amino function. Our findings permit to appropriately describe the atomic environment of the Si and Ti atoms at the short-range hybrid network, the formation of mixed phases, the interaction between the inorganic and the organic building blocks and their effect on the availability of aminopropyl groups at the pore surface. These basic structural aspects that derive from the sol-gel synthetic conditions are of paramount importance in the performance of these materials in a variety of applications such as adsorption, catalysis [47] or permselective molecular sorting [24, 46].

2 Experimental methods

2.1 Synthesis of mesoporous hybrid thin films

Mesoporous thin films were prepared by evaporation-induced self-assembly, using a block-copolymer template and a mixture of inorganic and hybrid precursors, following procedures previously described [45, 48, 49]. Initial solutions were prepared using tetraethoxysilane (TEOS) and $TiCl_4$ as inorganic precursors. APTES ($(CH_3CH_2O)_3Si(CH_2)_3NH_2$) was used to introduce the amino function through a co-condensation route [19]. Pluronics F127 block copolymer ($(EO)_{106}(PO)_{70}(EO)_{106}$, Aldrich) was used as a supramolecular template (EO: ethylene oxide-CH_2CH_2O-; PO: propylene oxide-$CH_2CH(CH_3)O$-). MilliQ water was added to trigger hydrolysis and extra acid was added to protonate the amino groups in solutions containing TEOS [50]. A set of precursor solutions was prepared varying the silica and titania precursor concentrations, keeping the organic function concentration constant in [APTES]/([TEOS] + [$TiCl_4$]) = 0.2. We have previously demonstrated that this concentration of amino functions leads to highly organized and accessible MHTF in the case of pure silica systems [34, 51]. Table 1 summarizes the precursor ratios for each solution, in the order in which they were slowly added under stirring (from left to right) into the final solutions. The hybrid film samples were labeled as A2SnTm (with $0 < n, m < 8$), representing the three precursors (A for aminosilica, S for the silicon alkoxide, T for the titanium chloride) in their nominal molar ratio. Below we use %Ti to indicate the fraction of Ti with respect to the total silica and titanium content expressed in percentage, ie. %Ti = T/(A + S + T)*100.

Synthesis mixtures were left under stirring at room temperature for two hours before thin film synthesis. Solutions prepared under these conditions were transparent and stable for at least 48 h at room temperature and can be reused several times by conserving them in a freezer at −20 °C, and gently restored to room temperature prior to dip-coating. The precursor solutions were used to produce mesoporous films by dip-coating on silicon wafers under 50% relative humidity (RH) at room temperature (1–2 mm s^{-1} withdrawing speed).

Table 1 Dipping solution compositions used to prepare hybrid mesoporous thin films

Sample Name	Reagent molar ratio						
	EtOH	$TiCl_4$	TEOS	APTES	F127	HCl	H_2O
A2S0T8	40	0.8	–	0.2	0.005	–	10
A2S2T6	36	0.6	0.2	0.2	0.005	0.07	8.8
A2S4T4	32	0.4	0.4	0.2	0.005	0.14	7.2
A2S6T2	28	0.2	0.6	0.2	0.005	0.21	6.4
A2S7T1	26	0.1	0.7	0.2	0.005	0.25	5.8
A2S8T0	24	–	0.8	0.2	0.005	0.28	5.2

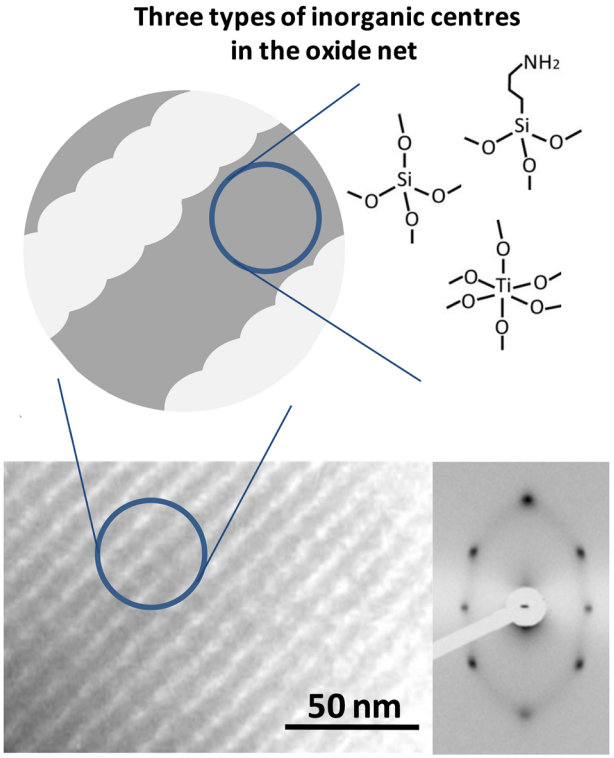

Fig. 1 Upper: Scheme showing the three types of inorganic centers in the mesoporous thin films. Lower: TEM image and (2D)-SAXS diffraction patterns of a typical film sample

Freshly deposited films were submitted to 50% RH chambers for 24 h, a stabilizing thermal treatment of two successive 24 h steps at 60 and 130 °C, and a final 2 h step at 200 °C. The template was eliminated by extraction in 0.01 mol dm^{-3} HCl in ethanol for three days, under stirring at 298 K. The mesostructure was conserved after the extraction process, as checked by 2D Small Angle X-Ray Scattering (2D-SAXS) and transmission electron microscopy (TEM); see Fig. 1.

In order to determine the effect of amino functions, purely inorganic oxide samples with equivalent Ti:Si composition were prepared as references (labeled SnTm) for comparison. These samples were prepared using the same conditions employed to prepare the hvbrid samples, excluding APTES from the dipping solution.

2.2 2D-SAXS and TEM characterization

Film mesostructure was characterized by 2D-SAXS at the D11A-SAXS2 line at the Laboratório Nacional de Luz Síncrotron, Campinas, SP, Brazil (LNLS), using $\lambda =$ 1.608 Å, a sample-detector distance of 650 mm, and a CCD detector at an incidence of 3°. TEM measurements were made using a Philips EM-301 TEM microscope using an acceleration voltage of 60 kV (Laboratorio de Microscopías Avanzadas, FCEN-UBA).

2.3 X-ray Photoelectron Spectroscopy (XPS)

XPS measurements were carried out using an Specs SAGE 150 system with a Mg K(alpha) (1253.6 eV) X-ray source and a 150 mm hemispherical electron energy analyzer. Quoted binding energies (BEs) are referenced to the adventitious C1s emission at 285 eV. Film composition was obtained from the integrated N 1s, Si 2p, and Ti 2p peak areas, after calibrating the equipment measuring different solid compounds of known stoichiometry. Repeated measurements were performed along the samples, confirming reproducible XPS line positions and intensity profiles with up to 2% accuracy. The mineral Si content of the samples (i.e., Si atoms not bonded to the aminopropyl functions) was estimated by substracting the Si signal of the A2S0T8 sample to the total Si signal of each sample. Further XPS measurements were performed at the D04A-SXS line of the LNLS, with a photon incident energy of 2500 eV using a 45° detection angle.

2.4 XANES characterization

Si K-XANES spectra were acquired in total electron yield mode by using an InSb(111) monochromator at the D04A-SXS beamline of the LNLS, Campinas, Brazil. The beam focalization was performed using a Ni mirror. The incident photon energy was in the range of 1820–2000 eV and energy resolution was about 1 eV. The incident beam intensity I_0 was measured using an Al thin foil located before the sample. Ti K-XANES experiments were performed at the A1 beamline of the DESY synchrotron, Hamburg, Germany, in transmition mode using two ion chambers as detectors. Energy range was 4920–5150 eV with an energy resolution of 1 eV. The photon energy was calibrated using a Si or Ti foil and setting the first inflection point to the energy of the K absorption edge of Si at 1839 eV and of Ti at 4966 eV. X-ray absorption data were analyzed using standard procedures: [52] two polynomial functions were fitted to substract the background and normalize the absorption spectrum, one for the pre-edge region (first-degree polynomial) and the other for the region above the edge (second-degree polynomial). After background subtraction and normalization, the white line region was fitted using Gaussian peaks. All spectra were fitted using WinXAS [53] to obtain the relative contribution from the fitted Gaussians in each spectrum.

3 Results and discussion

Thin films of mesoporous hybrid oxides based on a mixed SiO_2/TiO_2 framework containing aminopropyl groups were prepared by dip-coating in a one-pot strategy as described in

the Experimental Section. A set of samples were synthesized by varying the silica and titania precursor concentrations, keeping the organic function concentration constant (20 at% of organosilane). The expected final composition for these materials is $M_{0.8}(Si(CH_2)_3NH_2)_{0.2}O_{1.9}$ with M = Si and/or Ti (0% < Si, Ti < 80%, Si+Ti = 80%). These samples were labeled as A2S*n*T*m* (with $0 < n, m < 8$). Furthermore, thin oxide films without the aminopropyl functional group and with the same Ti:Si composition were prepared as references and were labeled SnTm.

All the obtained materials present highly organized mesoporous structures with cubic mesostructure since the same template precursor (Pluronic-F127) in a molar proportion $s = [F127]/([Ti]+[Si]) = 0.005$ was used. Figure 1 shows a representative TEM and 2D-SAXS pattern corresponding to highly organized regular pore arrays with cubic derived mesostructures (Im–3m symmetry, with the [110] plane oriented parallel to the substrate), uniaxially distorted in the *z* direction after the thermal stabilization treatment and template extraction. It is important to notice that samples deposited under 20% RH led to worm-like mesostructures. Typical contractions of about 40–50% are observed, i.e., pore height is about 6–8 nm and pore walls about 10 nm, in all samples (detailed SAXS information of all studied samples is presented in Fig. S1) [54, 55]. The TEM image shows that the inorganic framework is even and continuous and does not present dark regions corresponding to domains with Ti- or Si-rich segregation under the experimental conditions explored [56].

While the mesoporous mixed oxide structures present similar cubic mesostructures, significant differences are expected at the molecular level, due to the different Si:Ti atomic ratios. The pore wall structure can be described in a simplified manner as a three-dimensional M-O-M network (with M = Ti or Si centres) presenting short range order. Due to the mixed oxide frameworks and the low temperature of processing, these materials are mostly non-crystalline [44, 45], and the oxide network can be described as an amorphous system presenting three different types of inorganic centers (silicates, titanates and aminopropylsilicates) connected by oxo bridges (see scheme in Fig. 1). Each of these centers presents a specific geometry due to their interconnectivity, which will be analyzed and discussed in detail below.

XPS experiments were carried out in order to determine the chemical composition. We have previously shown that XPS provides representative information of the whole sample composition of MHTF samples due to their high accessible porosity and low thickness [34]. The elemental composition is summarized in Table 2 (details in Fig. S2). Clearly the nitrogen concentration, due to the presence of aminopropyl groups, remains practically constant at about 20% for all samples. Furthermore, the Silicate:Titanate ratio

Table 2 Quantitative XPS analysis of hybrid thin films samples with A2SnTm composition (see text)

	Inorganic Composition [%]		
	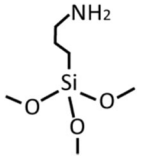	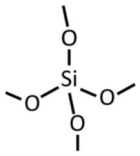	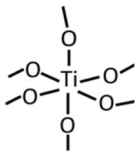
Name	N	mineral Si	Ti
A2S0T8	18	0	82
A2S2T6	22	17	61
A2S4T4	20	42	38
A2S6T2	20	62	18
A2S7T1	16	73	11
A2S8T0	19	81	0

Uncertainty of the data is lower than 5%, based in repeated measurements on each sample. The dominant amino, silicate and titanate species belonging to each element are sketched for an easier identification. See Fig. S2 for the detailed normalized integration

can be smoothly tuned in the range 0–80%. Finally, the elemental composition changes reproduces the nominal solution composition (see Experimental Section).

To investigate the local structure of the inorganic building blocks in A2SnTm hybrid materials synchrotron-based XANES measurements were performed. Figure 2A shows the Ti K-XANES spectra of an anatase TiO_2 reference compound (spectrum a) and of samples A2S2T6 (spectrum b), A2S6T2 (spectrum c), and A2S7T1 (spectrum d). Two regions can be discriminated, the pre-edge region (4965–4980 eV) shown in detailed in Fig. 2B and the white line region (4980–5020 eV) shown in detail in Fig. 2C. The pre-edge structures can be assigned as quadrupole transitions from the 1s core state to the empty 3d states [57]. When the inversion symmetry is broken, the pre-edge gains additional intensity, i.e., the pre-edge peak intensity for Td symmetry is larger than those for Oh symmetry for all 3d elements [58]. The XANES spectra presented in Fig. 2B display characteristic features in the pre-edge region, similar to crystalline-like TiO_2 structures for spectra a and b, and similar to expected for amorphous-like TiO_2 in spectra c and d [45]. Additional information can be obtained from the peak position and intensity in the pre-edge region. From the pre-edge XANES spectra of model compounds Farges et al. demonstrated that fourfold ($^{[4]}$Ti), fivefold ($^{[5]}$Ti) and sixfold ($^{[6]}$Ti) coordinated Ti result in a pre-edge peak with different position and height [59, 60]. Furthermore, from the comparison between the pre-edge spectra of mixtures of $^{[4]}$Ti, $^{[5]}$Ti and $^{[6]}$Ti model compounds and theoretical simulations they concluded that the pre-edge position and the normalized height should be used combined to determine the

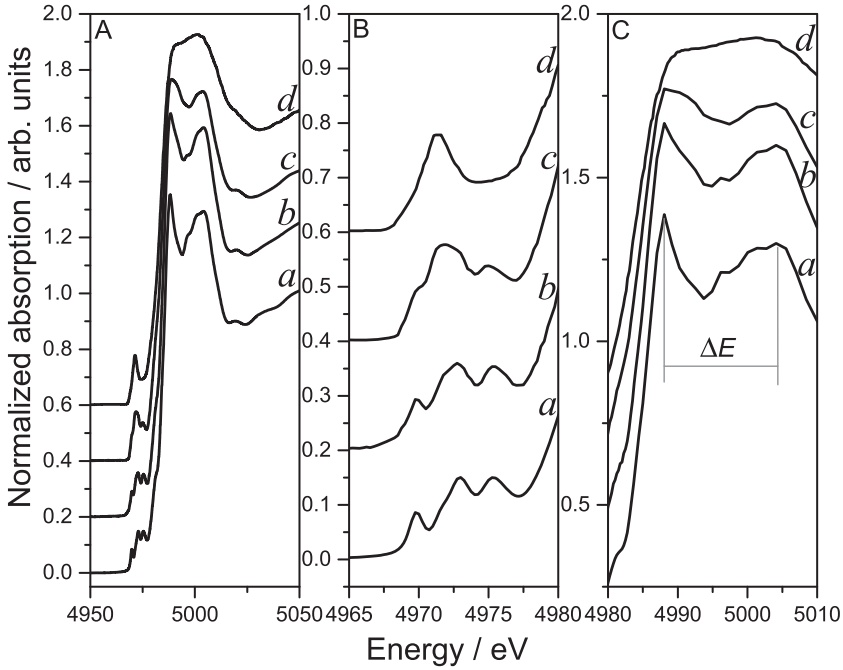

Fig. 2 **A** Ti K XANES spectrum of a TiO_2-anatase reference compound (a), A2S2T6 (b), A2S6T2 (c), A2S7T1 (d). **B** Detailed view of the pre-edge region associated with Ti-coordination. **C** Detailed view of the energy splitting (ΔE) in the white line region which can be used to estimate the Ti-O distance

contribution of each Ti coordination number. Inserting the peak positions and heights obtained from the spectra in Fig. 2B into the coordination diagram proposed by Farges et al. [59, 60]. indicates that a mixture of $^{[4]}Ti + {}^{[6]}Ti$ is present in all A2SnTm samples, with a ratio $^{[4]}Ti\ /^{[6]}Ti < 0.5$ and with no $^{[5]}Ti$.

The white line region shows an evident energy splitting ΔE (Fig. 2C) that changes as the Ti composition increases. This energy difference ΔE changes with the distance between absorbing atoms and their ligands according to Natoli's rule [61, 62]:

$$r_{(Ti-O)} = c.(1/\Delta E)^{1/2} \quad (1)$$

where $r_{(Ti\text{-}O)}$ is the distance between Ti and O atoms, and c is a constant. Figure 3 shows changes in Ti–O distances as a function of the Ti fraction on the A2SnTm samples (left side, solid symbols). For comparison, a set of inorganic oxide samples (without the aminopropyl functional groups), called SnTm, were measured as reference compounds (right side, open symbols). These reference compounds are also mesoporous thin films based on mixed oxide frameworks $SiO_2 + TiO_2$ prepared in the absence of aminopropyl groups, with a systematic variation of silica and titania precursor concentrations. The expected chemical composition for the reference samples is $Ti_xSi_{1-x}O_2$ ($0 < x < 1$). The synthesized films present a cubic derived mesostructure, as we have reported previously [45]. Note that Ti-O distances were normalized with respect to the Ti-O distance in the anatase structure, $r_{anatase}$ [63].

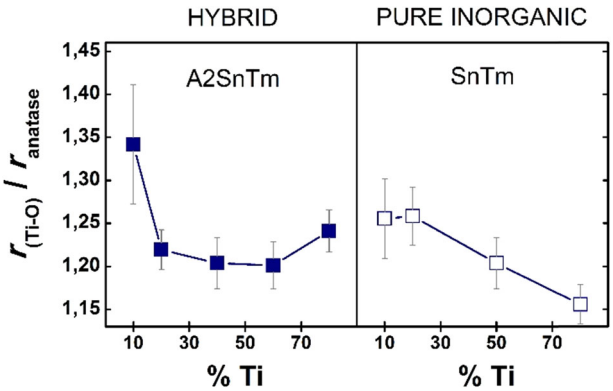

Fig. 3 Ti K-edge analysis for hybrid thin films A2SnTm (left side, solid symbols) and pure inorganic materials (right side, open symbols). The normalized Ti-O distance respect to anatase (up), $r_{(Ti\text{-}O)}/r_{anatase}$ is plotted as a function of titania centers concentration. %Ti represents the fraction of Ti with respect to the total silica and titanium content expressed in percentage, ie. %Ti = T/(A + S + T)*100

Figure 3 shows that the inclusion of an aminopropyl functional group by co-condensation alters the local environment of Ti, reflected in a change in trends in the Ti-O distances for higher Ti contents. Particularly, the comparison of Ti-O distances between the sets of A2SnTm and SnTm samples indicates that:

(a) Regarding purely inorganic SnTm thin films, Ti-O distances decrease with increasing %Ti, as expected. Ti-richer samples become more similar to pure titania, where Ti-O distances are shorter. Similar results were

previously obtained for mesoporous silica-titania mixed oxides calcined at higher temperatures, where the Ti-O distance became closer to the anatase values as the Ti content was increased, due to the higher crystalline character on those samples [45].

(b) In hybrid samples, the trend is different. For low-Ti content (A2S7T1) the Ti-O distance is longer than any distance observed in the absence of the aminopropyl functional group. In the intermediate range (20 < 80% Ti), the Ti-O distances are comparable to those observed in the corresponding oxides of intermediate composition, being practically invariant except for a slight variation at the higher %Ti values. This difference in behaviour suggests that the presence of aminopropyl silicates in the starting sols or in the freshly formed oxide network may induce the formation of a new type of phase with a high degree of Si-O-Ti interdispersion. This is reflected in an extended silica-titania interface with longer Ti-O distances in average. These longer distances are characteristic of a more amorphous titania [45]. In the A2S0T8 sample that contains no mineral silica, the Ti-O distance is substantially larger than the distance obtained in the comparable oxide material. This suggests that the organic functions somehow assist the dispersion of the Ti centers preventing extended crystalline titania nucleation, which is in agreement with the XPS and Si-K XAS experiments presented and discussed below.

XPS analysis of O1s spectra provides a sensitive tool to characterize the intermixing of SiO_2 and TiO_2. In particular, previous studies of inorganic mixed silica-titania oxide powders have shown that the O1s binding energies (BE) of SiO_2 and TiO_2 are significantly different (532.9 and 530 eV, respectively). Furthermore, in mixed oxide compounds, intermediate O 1s BE values around 531 eV can be attributed to oxygen atoms in Si-O-Ti bonds [64, 65].

Figure 4 shows O 1s spectra of the following hybrid samples: A2S6T2 (%Ti = 20), A2S4T4 (%Ti = 40) and A2S2T6 (%Ti = 60). Vertical dotted lines can be mainly attributed to the O 1s BE of SiO_2, Si-O-Ti and TiO_2. The presence of hydroxyl groups is expected at 1.5 eV higher binding energies with respect to the oxide components [66]. Thus, although we cannot rule out the presence of surface Si-OH or Ti-OH groups, their contribution to the total signal is very small and does not affect the interpretation of the data. Clearly, as the fraction of Ti in the films increases (and the Si fraction decreases) the intensity of the Si-O contribution decreases as expected. However, increasing the Ti content does not result in a corresponding increase in the Ti-O contribution to the O 1s spectra, instead a large increase in the Si-O-Ti contribution is observed. This differs from

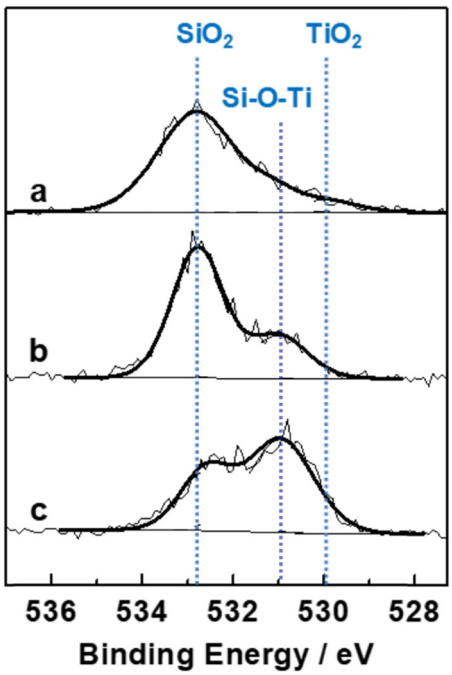

Fig. 4 O1s XPS spectra of hybrid thin films: A2S6T2 (**a**), A2S4T4 (**b**) and A2S2T6 (**c**)

the behaviour of silica:titania mixed films where increasing the Ti content increased the degree of Ti-O bonds, as the Ti-O distance became closer to the anatase distance (see Fig. 3). This reinforces the argument that the presence of the aminopropyl functional group in the hybrid mixed mesoporous thin films favours the interdispersion of the Ti centers resulting in the formation of Si-O-Ti bonds. Finally we note that an appreciably high fraction of Si-O-Si bonds is present in all A2SnTm films, which could be due to the presence of Si-O-Si or Si-O-Si(R) nanodomains.

For further structural characterizations of the Si species, we performed XANES experiments at the Si K-edge. Figure 5A shows XANES Si K-edge spectra of the different A2SnTm thin films. This region of the spectrum corresponds to the dipolar transition 1s → t2(Si 3p–3s) and provides information of the Si(IV) coordination geometry [67]. The strong absorption at 1846.8 eV represents a typical feature for the tetrahedrically coordinated Si in silica matrices. A first inspection of the spectra intensity and shape changes indicates that the Si coordination geometry is altered between the different samples. Particularly, in the spectrum corresponding to the sample with no mineral silica (A2S0T8) this feature is not the most intense as in the rest of the samples; in this sample, the intensity of the first electronic transition is the highest one. The same distinctive feature was previously observed in isolated asymmetric organosilanes [68] which are similar to the organic building block precursor used in our synthesis.

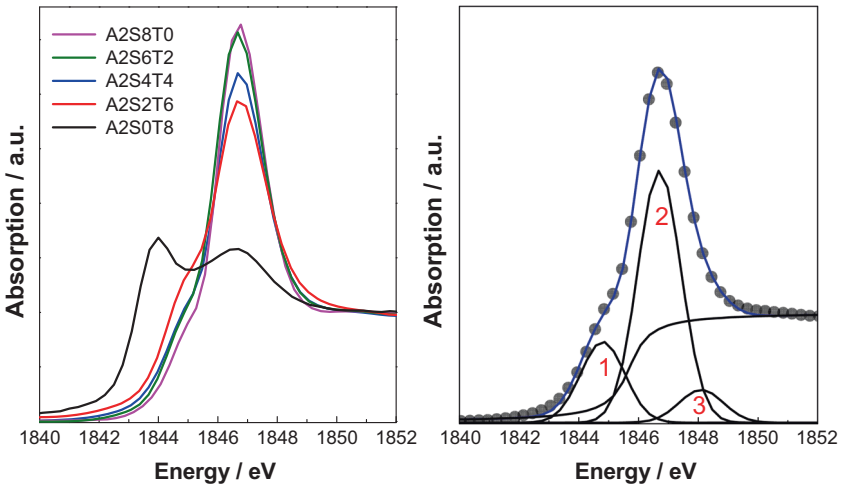

Fig. 5 Si K-edge XANES spectra for hybrid A2SnTm thin film samples. Left: Normalized XANES spectra for all samples. Right: Example of the peak deconvolution analysis using three components (black lines) of the A2S4T4 sample (black circles) (see text). Peak 1 is associated to the forbidden transition $1\,s \rightarrow a_1$ (Si 3s-3p), peak 2 to the $1s \rightarrow t_2$ (Si 3p-3s) $^{[4]}$Si transition and peak 3 to the $1\,s \rightarrow t_2$ (Si 3p-3s) $^{[6]}$Si transition

A complete reproduction of the Si K-XANES spectra can be obtained fitting with three Gaussian curves, as depicted in Fig. 5B. The first contribution (1), centered at 1844.6 eV, is attributed to the forbidden electronic transition $1\,s \rightarrow a_1$ (Si 3s-3p), which can be associated with a loss of symmetry in tetrahedral Si coordination and is labeled $^{[4]}Si_{asym}$ [69]. The second peak (2), centered at 1846.8 eV, corresponds to the white line, associated with the $1\,s \rightarrow t_2$ (Si 3p-3s) transition in tetrahedral Si and is labeled $^{[4]}$Si [67]. A third contribution (3) at 1848.3 eV, is also associated with the $1\,s \rightarrow t_2$ (Si 3p-3s) transition but for octahedrally coordinated Si and is labeled $^{[6]}$Si [64].

A first analysis of the Gaussian fitted peak areas of the Si K edge spectra signals 1, 2, and 3 mentioned above, assigned respectively to $^{[4]}Si_{asym}$, $^{[4]}$Si and $^{[6]}$Si permits to identify two simple trends (see Fig. S4). In the mixed oxides, a marked decrease in the $^{[4]}$Si signal is observed with increasing the Ti contents, up to 30% Ti; this is reflected at the same time in a fast increase in the asymmetric and octahedral Si signals ($^{[4]}Si_{asym}$ and $^{[6]}$Si). For higher %Ti, changes are still observed, albeit less marked. These results demonstrate that increasing the Ti(IV) content leads to substantial changes in the Si coordination for %Ti < 30%, notably an increase in the Si average coordination (appearance of octahedral Si) and an increase in the asymmetry of the Si tetrahedral sites, part of which can be ascribed to the formation of Si-O-Ti bonds. These two aspects have already been observed in mixed mesoporous silica-titania oxides treated to high temperatures and attributed to a high Si-Ti interdispersion [45]. For %Ti < 30%, the changes are less marked; this is in agreement with the formation of Ti-oxo domains with shorter Ti-O distance evidenced by Ti-K XANES analysis. It seems that, under these synthesis conditions (mild thermal treatment, template extraction by solvent), titania clusters can phase separate for high %Ti.

In the hybrid materials, as in purely inorganic oxides, a continuous decrease in the $^{[4]}$Si signal with increasing %Ti is observed (see Figs. S4 and S5 in supplementary information). However, three changes with respect to pure inorganic oxides are evident: (a) a lower initial $^{[4]}$Si fraction, and a more marked decrease along increasing Ti presence, (b) a stronger increase in the $^{[4]}Si_{asym}$ signal, (c) the fraction of octahedral sites keeps relatively constant or slightly decreasing. The marked differences in the Si coordination are again visible and attributable to the presence of the organosilane. The lower initial $^{[4]}$Si fraction in the hybrid samples with respect to the oxides is due to the presence of the APTES precursor. The decrease in the $^{[4]}$Si sites along %Ti is compensated with an important increase in the $^{[4]}Si_{asym}$ signal, which increases much more than in the case of the mixed oxides. We can assign this asymmetric signal mostly to the APTES fragments in the hybrid samples, although a fraction of this signal may be due to the asymmetry of the mineral Si centers connected with Ti centres, as discussed above. This difference with respect to the oxides can be also attributed to the interdispersion of the Ti centres in the hybrid material.

The $^{[6]}$Si signal in the XANES spectra of the hybrid materials can be attributed both to octahedrally coordinated silicon atoms due to the substitution of Ti by Si in the titania network (as observed in the oxides, see above) and to the presence of functional organic groups affecting the Si environment. Indeed, a fraction of the signal $^{[6]}$Si signal in the hybrid materials may be a consequence of the presence of Si-C bonds. It has been observed that the partial substitution of Si-O bonds by Si-C or Si-N gives rise to the appearance of an intense pre-peak in the Si K-edge XANES [70, 71]. In particular, Chaboy et al. showed that while there is a substitution of C by O in the Si environments, there is also a modification of the interatomic distances in a tetrahedral arrangement; these distortions can lead to

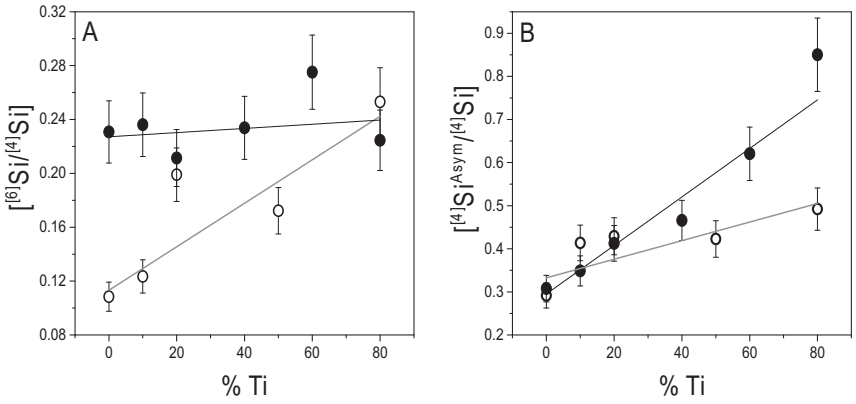

Fig. 6 Si K-XANES peak analysis of the octahedral: tetrahedral (**A**) and asymmetric tetrahedral: tetrahedral signal ratio (**B**) for mesoporous hybrid thin films A2SnTm (solid symbols) and pure inorganic mesoporous materials SnTm (open symbols). % Ti represents the fraction of Ti with respect to the total silica and titanium content expressed in percentage, i.e., %Ti = T/(A + S + T)*100

absorptions above the white line. Following this interpretation, we can attribute at least a fraction of the $^{[6]}$Si signal of the hybrids to the increasingly important presence of Si-C bonds as the amount of Ti increases. Interestingly, for a sample with no mineral Si centers (A2S0Ti8), the signal associated to the octahedral sites shows a slight decrease of the order of 20%, with a marked appearance of the $^{[4]}Si_{asym}$ signal.

The effect of sample composition on the Si coordination geometry is shown in Fig. 6 where the peak area ratios corresponding to different Si coordination geometries is plotted as a function of %Ti for the MHTF (solid symbols) and for reference SnTm inorganic films (open symbols). Figure 6A shows the [$^{[6]}$Si]/[$^{[4]}$Si] ratio, determined by the ratio between areas of peaks 3 and 2 in the Si K-XANES spectra (see Fig. 5B), as a function of %Ti. This figure shows that most of the Si centers are $^{[4]}$Si with a minor fraction of $^{[6]}$Si in all samples. In addition, the intensity ratio indicates a higher fraction of $^{[6]}$Si in the hybrid films with Ti content greater than 20% as compared with the SnTm films. As discussed above, this seems to indicate that the amino functions contribute to increasing the average coordination of mineral Si centres in the titania-silica matrix. Figure 6B shows the [$^{[4]}$Si^{asym}]/[$^{[4]}$Si] ratio, determined by the ratio of peaks 1 and 2 in the Si K-XANES spectra, as a function of %Ti. Clearly, the average environment of tetrahedral Si in the hybrid materials is always more asymmetric than in pure inorganic samples due to the presence of the aminopropyl-group that breaks the Td symmetry.

Overall the Si K-XANES spectra shows that the population of the $^{[6]}$Si sites is more or less constant with Ti(IV) in the hybrid films with respect to the mixed oxide materials, reflecting the presence and the role of the organic groups. On the contrary, the fourfold coordinated $^{[4]}Si_{asym}$ species grow at the expense of the symmetric tetrahedral sites, in a more marked way than the one observed in the oxides (see Fig. S4). These observations agree with the increased formation of a mixed silica-titania oxide phase with increasing %Ti observed in the hybrid samples both by the Ti-K XANES and XPS measurements discussed above (see Fig. 4). These experiments are also consistent with smaller Ti-oxo (i.e., more amorphous) domains in the presence of the organosilane.

The structure of the mixed phases formed here should be a consequence of the sol-gel processes taking place upon film deposition, because the mesoporous materials were obtained in relatively mild conditions (200 °C treatment followed by template extraction). In the starting water-ethanol solutions, three precursors with very dissimilar reactivity are present. It has been demonstrated that in the water-rich conditions employed here, $TiCl_4$ has a very fast hydrolysis rate that leads to highly acidic solutions, where condensation is arrested and therefore small, cluster-like titania species are formed that self-assemble with the templates upon drying [72, 73]. This acidic medium can assist TEOS hydrolysis and partial condensation. On the other hand, the protons released by $TiCl_4$ hydrolysis are enough to protonate APTES. This last effect hinders the possible nucleophilic attack of TEOS precursors by the amino group. Therefore, on the basis of the reactivity of the synthesis precursors, we can suggest that the mixed silica-titania phases are grown from the reaction between Ti(IV) clusters, and hydrolyzed or mildly condensed silica species such as Si-oxo olygomers containing protonated APTES fragments [74]. Protonated APTES could act in this case as a compatibilizer between silica and titania precursors, generating an enhanced interface. In this context, the presence of titanates could also influence the interactions and linkages between the aminosilicate species and the M-oxo networks, influencing in turn the availability of the amino groups.

The effect of composition and the organization of the inorganic centers on the hybrid oxide structure at the surface of the materials was studied following the protonation of the aminopropyl functional groups with XPS. As described in

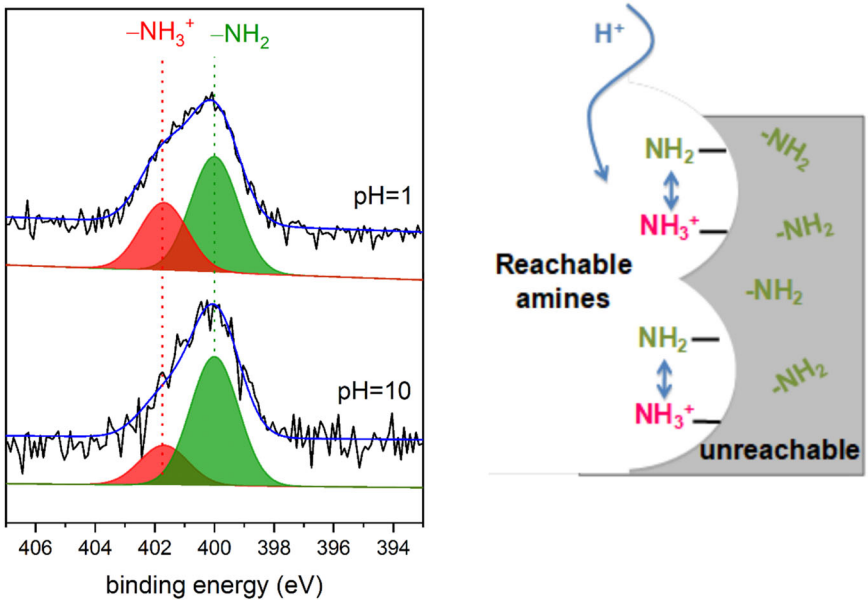

Fig. 7 On the left, N 1s XPS spectra of A2S0T8 hybrid thin film exposed to acid (pH = 1) and alkaline (pH = 10) medium. On the right, scheme of hybrid pore wall indicating the reachable and unreachable amines (see text)

the previous sections, all A2SnTm hybrid thin films show the same concentration of organic groups, i.e., 20% of aminopropylsilane. However, due to the co-condensation method used, the aminopropyl groups can be roughly divided in two different classes, as schematized in Fig. 7 [51]. The first class is constituted by amine groups that are buried into the mixed oxide matrix, and cannot exchange protons, which will be labeled "unreachable amines". The second class is represented by amine groups that are dangling into the pore cavity and readily exchange protons, which will be called "reachable amines".

XPS experiments were performed after film immersion in pH = 1 and pH = 10 solutions to distinguish spectroscopically reachable and unreachable amines. Figure 7 shows the N1s XPS spectra of A2S0T8 at pH = 1 (top spectrum) and at pH = 10 (bottom spectrum). In both cases, the N1s XPS signal contains two components at 402 and 400 eV. These peaks are due to protonated ($-NH_3^+$) and unprotonated ($-NH_2$) amine groups respectively [75]. Clearly, the $-NH_2$ contribution at 400 eV is the main peak contribution and the area of the signal corresponding to $-NH_3^+$ increases for samples treated at pH = 1. This implies that a significant number of amines were not reached by protons at pH = 1. This is, only a small group of amines are able to be protonated at pH = 1. We can estimate the percentage of "reachable amines" from the difference between the NH_3^+/NH_2 ratios at the pH = 1 and pH = 10: [51]

$$\%\,\text{Reachable Amines} = \left\{ \left(\frac{\text{area} - \text{NH}_3^+}{\text{area} - \text{NH}_2} \right)_{\text{pH}=1} - \left(\frac{\text{area} - \text{NH}_3^+}{\text{area} - \text{NH}_2} \right)_{\text{pH}=10} \right\} \text{x } 100 \quad (2)$$

Table 3 Percentage of reachable amines in A2SnTm hybrid materials as a function of %Ti

Sample name	% Ti	% Reachable amines
A2S2T6	60	16
A2S4T4	40	22
A2S6T2	20	21
A2S7T1	10	19
A2S8T0	0	7

Table 3 shows the percentage of reachable amine groups as a function of Ti content for different A2SnTm samples. Note that: (a) the pure silica sample A2S8T0 shows less than 10% of reachable amines groups and (b) the addition of Ti(IV)centers (from 10–80%) increases significantly the reachable amine percentage; this value increases drastically even for small Ti(IV) additions, and remains constant at ca. 20% for the rest of the samples.

Thus, the presence of Ti(IV) centers in the hybrid network favours the surface availability of the organic functional group, but a small amount of these centers saturates this effect, leading to a similar number of reachable amines in samples with 10–80% of titanates. Taking into account the previous discussion on the role of Ti(IV) centers in the APTES protonation, we propose that the interaction of the protonated aminopropylsilicates with silica oligomers could be smaller when Ti is absent, and that the presence of $^{[6]}$Ti octahedrically coordinated (anatase-like geometry) might assist a preferable location of aminated residues near the pore surface. This observation stresses the important role of transition metal ions in the development of hybrid oxide networks.

4 Conclusions

The combination of Ti and Si K-XANES and XPS measurements provides information about the local structure around Ti and Si atoms and chemical speciation in mixed oxide-based mesoporous hybrid thin films. Mixed silica and titania mesoporous thin films containing aminopropyl functional groups present a higher average coordination number for Ti atoms than the pure inorganic materials. For Ti concentration in the order of 10%, Ti(IV) is likely in a low coordination state, well dispersed within a silica matrix; octahedral Ti centers ($^{[6]}$Ti) with relatively long Ti-O bonds are observed from low Ti concentration (about 20%) in the hybrid materials, while in the mixed oxide phases, small Ti-oxo domains with shorter bonds are formed. The looser coordination of Ti atoms in the hybrid phase is most probably due to the formation of a mixed oxide phase, as demonstrated by the XPS experiments. This is assisted by the binding between Si-organic and inorganic centers, rather than being due to phase segregation of pure titania within the hybrid structure. In turn, the Si-K XANES experiments clearly show both silica-titania intermixing and an increase in the deformation of the silica tetrahedral symmetry concurrent with the titania increase. Aminopropyl species may act as a compatibilizer among the titanate and mineral silica centers.

The addition of Ti seems to assist the availability of amino groups on the pore surface, which is probably associated to the faster hydrolysis and condensation of TEOS due to the presence of the highly acidic $TiCl_4$ in the precursor solutions. This higher acidity leads to more protonated ammonium groups, which aids their exposure at the inorganic framework-template interface, even in the presence of only 10% of titanates.

In summary, our study based in crossed XANES and XPS characterization provides a means to obtain quantitative structural information of a complex mesoporous material that presents different functions present within the walls and also on the pore surface. The location of these functions depends on the interplay between the added amino function and the formation kinetics of the inorganic scaffolds to yield nanostructured mixed oxides. We thus can provide significant information for the rational design of organic-inorganic materials, useful for the subsequent functionalization required for applications based on the framework and surface properties of mesoporous hybrid materials. Interestingly, understanding the sol-gel aspects and the assembly processes that take place in film formation permits to extrapolate these interesting systems, presenting three different functional groups to xerogels, aerogels or aerosols, which can be of interest in catalysis, molecular sieving or tissue engineering.

Data availability

Supplementary Data are available at the Publisher.

Acknowledgements This work was funded by CONICET (PIP No. 112-201101-01035) and ANPCyT (PICT 2017-4651, PICT 2017-1220, PICT 2018-04236, PICT 2018-03276). Synchrotron measurements were possible thanks to funding from LNLS, Campinas, Brazil: 2D SAXS (line D11A-SAXS1 Project Nos. 5867/06 and 6721/07) and XANES (line D04A-SXS Project Nos. 10808/11 and 15187/13).

Compliance with ethical standards

Conflict of interest The authors declare no competing interests.

Publisher's note Springer Nature remains neutral with regard to jurisdictional claims in published maps and institutional affiliations.

References

1. Kickelbick G (2007) Hybrid materials: synthesis, characterization, and applications. WILEY-VCH Verlag
2. Nicole L, Boissiere C, Grosso D et al. (2005) Mesostructured hybrid organic-inorganic thin films. J Mater Chem 15:3598–3627. https://doi.org/10.1039/B506072A
3. Sanchez C, Belleville P, Popall M, Nicole L (2011) Applications of advanced hybrid organic–inorganic nanomaterials: from laboratory to market. Chem Soc Rev 40:696–753. https://doi.org/10.1039/c0cs00136h
4. Faustini M, Nicole L, Ruiz-Hitzky E, Sanchez C (2018) History of organic–inorganic hybrid materials: prehistory, art, science, and advanced applications. Adv Funct Mater 28. https://doi.org/10.1002/adfm.201704158
5. Ruiz-Hitzky E, Wicklein B (2018) The fascinating world of the functional hybrid and biohybrid materials. Adv Funct Mater 28:1803407. https://doi.org/10.1002/adfm.201803407
6. Park SS, Ha C-S (2018) Hollow hybrid materials: hollow mesoporous functional hybrid materials: fascinating platforms for advanced applications. Adv Funct Mater 28:1870183. https://doi.org/10.1002/adfm.201870183
7. Margelefsky EL, Zeidan RK, Davis ME (2008) Cooperative catalysis by silica-supported organic functional groups. Chem Soc Rev 37:1118–1126. https://doi.org/10.1039/b710334b
8. Climent MJ, Corma A, Iborra S (2011) Heterogeneous catalysts for the one-pot synthesis of chemicals and fine chemicals. Chem Rev 111:1072–1133. https://doi.org/10.1021/cr1002084
9. Díaz U, Brunel D, Corma A (2013) Catalysis using multifunctional organosiliceous hybrid materials. Chem Soc Rev 42:4083–4097. https://doi.org/10.1039/c2cs35385g
10. Fernandes AE, Jonas AM (2019) Design and engineering of multifunctional silica-supported cooperative catalysts. Catal Today 334:173–186. https://doi.org/10.1016/j.cattod.2018.11.040
11. Notestein JM, Katz A (2006) Enhancing heterogeneous catalysis through cooperative hybrid organic-inorganic interfaces. Chem - A Eur J 12:3954–3965. https://doi.org/10.1002/chem.200501152
12. Motokura K, Tada M, Iwasawa Y (2007) Heterogeneous organic base-catalyzed reactions enhanced by acid supports. J Am Chem Soc 129:9540–9541. https://doi.org/10.1021/ja0704333
13. Motokura K, Tada M, Iwasawa Y (2008) Cooperative catalysis of primary and tertiary amines immobilized on oxide surfaces for one-pot C-C bond forming reactions. Angew Chem—Int Ed 47:9230–9235. https://doi.org/10.1002/anie.200802515

14. Motokura K, Tada M, Iwasawa Y (2009) Layered materials with coexisting acidic and basic sites for catalytic one-pot reaction sequences. J Am Chem Soc 131:7944–7945. https://doi.org/10.1021/ja9012003
15. Soler-Illia GJAA, Azzaroni O (2011) Multifunctional hybrids by combining ordered mesoporous materials and macromolecular building blocks. Chem Soc Rev 40:1107–1150. https://doi.org/10.1039/c0cs00208a
16. Innocenzi P, Malfatti L (2013) Mesoporous thin films: properties and applications. Chem Soc Rev 42:4198–4216. https://doi.org/10.1039/c3cs35377j
17. Lebeau B, Galarneau A, Linden M (2013) Introduction for 20 years of research on ordered mesoporous materials. Chem Soc Rev 42:3661–3662. https://doi.org/10.1039/c3cs90005c
18. Brilmayer R, Förster C, Zhao L, Andrieu-Brunsen A (2020) Recent trends in nanopore polymer functionalization. Curr Opin Biotechnol 63:200–209. https://doi.org/10.1016/j.copbio.2020.03.005
19. Soler-Illia GJAA, Innocenzi P (2006) Mesoporous hybrid thin films: the physics and chemistry beneath. Chem—Eur J 12. https://doi.org/10.1002/chem.200500801
20. Innocenzi P, Soler-Illia G (2009) Mesoporous thin films: an example of pore engineered material. Key Eng Mater 391:109–120. https://doi.org/10.4028/www.scientific.net/KEM.391.109
21. Soler-Illia GJAA, Vensaus P, Onna D (2021) Chemical methods to produce mesoporous thin films with tunable properties. In: Das S, Dhara S (eds) Chemical solution synthesis for materials design and thin film device applications. Elsevier, pp 195–229. https://doi.org/10.1016/B978-0-12-819718-9.00002-9
22. Nasir T, Herzog G, Hébrant M et al. (2018) Mesoporous silica thin films for improved electrochemical detection of paraquat. ACS Sens 3:484–493. https://doi.org/10.1021/acssensors.7b00920
23. Otal EH, Angelomé PC, Bilmes SA, Soler-Illia GJAA (2006) Functionalized mesoporous hybrid thin films as selective membranes. Adv Mater 18. https://doi.org/10.1002/adma.200502215
24. Alberti S, Soler-Illia GJAA, Azzaroni O (2015) Gated supramolecular chemistry in hybrid mesoporous silica nanoarchitectures: Controlled delivery and molecular transport in response to chemical, physical and biological stimuli. Chem Commun 51:6050–6075. https://doi.org/10.1039/c4cc10414e
25. Calvo A, Yameen B, Williams FJ, et al. (2009) Facile molecular design of hybrid functional assemblies with controllable transport properties: Mesoporous films meet polyelectrolyte brushes. Chem Commun. https://doi.org/10.1039/b822489g
26. Calvo A, Yameen B, Williams FJ et al. (2009) Mesoporous films and polymer brushes helping each other to modulate ionic transport in nanoconfined environments. An interesting example of synergism in functional hybrid assemblies. J Am Chem Soc 131:10866–10868. https://doi.org/10.1021/ja9031067
27. Silies L, Andrieu-Brunsen A (2018) Programming ionic pore accessibility in zwitterionic polymer modified nanopores. Langmuir 34:807–816. https://doi.org/10.1021/acs.langmuir.7b00529
28. Andrieu-Brunsen A, Micoureau S, Tagliazucchi M et al. (2015) Mesoporous hybrid thin film membranes with PMETAC@Silica architectures: controlling ionic gating through the tuning of polyelectrolyte density. Chem Mater 27:808–821. https://doi.org/10.1021/cm5037953
29. Rafti M, Brunsen A, Fuertes MC et al. (2013) Heterogeneous catalytic activity of platinum nanoparticles hosted in mesoporous silica thin films modified with polyelectrolyte brushes. ACS Appl Mater Interfaces 5:8833–8840. https://doi.org/10.1021/am403836f
30. Calvo A, Fuertes MC, Yameen B et al. (2010) Nanochemistry in confined environments: polyelectrolyte brush-assisted synthesis of gold nanoparticles inside ordered mesoporous thin films. Langmuir 26:5559–5567. https://doi.org/10.1021/la9038304
31. Yang Q, Li C (2014) Catalysis in porous-material-based nanoreactors: a bridge between homogeneous and heterogeneous catalysis. In: Can L, Yan L (eds) Bridging heterogeneous and homogeneous catalysis: concepts, strategies, and applications. WILEY-VCH Verlag, pp 351–396
32. Chandra P, Jonas AM, Fernandes AE (2018) Sequence and surface confinement direct cooperativity in catalytic precision oligomers. J Am Chem Soc 140:5179–5184. https://doi.org/10.1021/jacs.8b00872
33. Goettmann F, Sanchez C (2007) How does confinement affect the catalytic activity of mesoporous materials? J Mater Chem 17:24–30. https://doi.org/10.1039/b608748p
34. Calvo A, Angelomé PC, Sánchez VM et al. (2008) Mesoporous aminopropyl-functionalized hybrid thin films with modulable surface and environment-responsive behavior. Chem Mater 20:4661–4668. https://doi.org/10.1021/cm800597k
35. Puglisi A, Annunziata R, Benaglia M et al. (2009) Hybrid inorganic-organic materials carrying tertiary amine and thiourea residues tethered on mesoporous silica nanoparticles: synthesis, characterization, and co-operative catalysis. Adv Synth Catal 351:219–229. https://doi.org/10.1002/adsc.200800635
36. Brunelli NA, Venkatasubbaiah K, Jones CW (2012) Cooperative catalysis with acid-base bifunctional mesoporous silica: impact of grafting and Co-condensation synthesis methods on material structure and catalytic properties. Chem Mater 24:2433–2442. https://doi.org/10.1021/cm300753z
37. Lauwaert J, Moschetta EG, Van Der Voort P et al. (2015) Spatial arrangement and acid strength effects on acid-base cooperatively catalyzed aldol condensation on aminosilica materials. J Catal 325:19–25. https://doi.org/10.1016/j.jcat.2015.02.011
38. Manangon-Perugachi LE, Smeets V, Vivian A, et al. (2021) Mesoporous methyl-functionalized titanosilicate produced by aerosol process for the catalytic epoxidation of olefins. https://doi.org/10.3390/catal11020196
39. Bianconi A, Incoccia L, Stipcich S (1983) EXAFS and near edge structure. Springer-Verlag, Berlin
40. van Bokhoven JA, Lamberti C (2015) X-ray absorption and x-ray emission spectroscopy: theory and applications
41. Jiang N, Su D, Spence JCH (2007) Determination of Ti coordination from pre-edge peaks in Ti K -edge XANES. Phys Rev B - Condens Matter Mater Phys 76. https://doi.org/10.1103/PhysRevB.76.214117
42. Wu Z, Xian DC, Natoli CR et al. (2001) Symmetry dependence of X-ray absorption near-edge structure at the metal K edge of 3d transition metal compounds. Appl Phys Lett 79:1918–1920. https://doi.org/10.1063/1.1405149
43. Angelomé PC, Andrini L, Calvo ME et al. (2007) Mesoporous anatase TiO_2 films: Use of Ti K XANES for the quantification of the nanocrystalline character and substrate effects in the photocatalysis behavior. J Phys Chem C 111:10886–10893. https://doi.org/10.1021/jp069020z
44. Andrini L, Angelomé PC, Soler-Illia GJAA, Requejo FG (2016) Understanding the Zr and Si interdispersion in Zr1-xSixO2 mesoporous thin films by using FTIR and XANES spectroscopy. Dalt Trans 45:9977–9987. https://doi.org/10.1039/c6dt00203j
45. Angelomé PC, Andrini L, Fuertes MC et al. (2010) Large-pore mesoporous titania-silica thin films (Ti1-xSixO2, $0.1 \leq x \leq 0.9$) with highly interdispersed mixed oxide frameworks. Comptes Rendus Chim 13:256–269. https://doi.org/10.1016/j.crci.2009.07.001
46. Calvo A, Angelomé PC, Sánchez VM et al. (2008) Mesoporous aminopropyl-functionalized hybrid thin films with modulable surface and environment-responsive behavior. Chem Mater 20:4661–4668. https://doi.org/10.1021/cm800597k
47. Zhang JF, Wang ZM, Lyu YJ et al. (2019) Synergistic catalytic mechanism of acidic silanol and basic alkylamine bifunctional

groups over SBA-15 Zeolite toward aldol condensation. J Phys Chem C 123:4903–4913. https://doi.org/10.1021/acs.jpcc.8b11941
48. Angelomé PC, Soler-Illia GJDAA (2005) Ordered mesoporous hybrid thin films with double organic functionality and mixed oxide framework. J Mater Chem 15:3903–3912. https://doi.org/10.1039/b506484h
49. Soler-Illia GJAA, Angelomé PC, Bozzano P (2004) Highly ordered hybrid mesoporous bifunctional thin films. Chem Commun 2854. https://doi.org/10.1039/b413260b
50. Cagnol F, Grosso D, Sanchez C (2004) A general one-pot process leading to highly functionalised ordered mesoporous silica films. Chem Commun 4:1742–1743. https://doi.org/10.1039/b403753g
51. Calvo A, Joselevich M, Soler-Illia GJAA, Williams FJ (2009) Chemical reactivity of amino-functionalized mesoporous silica thin films obtained by co-condensation and post-grafting routes. Microporous Mesoporous Mater 121:67–72. https://doi.org/10.1016/j.micromeso.2009.01.005
52. Durham PJ (1987) Theory of XANES. In: Koningsberger DC, Prins R (eds) X-ray absorption: principles, applications, techniques of EXAFS, SEXAFS. Wiley, New York, NY, p 53–84
53. Ressler T (1998) WinXAS: a program for X-ray absorption spectroscopy data analysis under MS-Windows. J Synchrotron Radiat 5:118–122. https://doi.org/10.1107/S0909049597019298
54. Soler-Illia GJAA, Crepaldi EL, Grosso D, et al. (2002) Structural control in self-standing mesostructured silica oriented membranes and xerogels. Chem Commun 2. https://doi.org/10.1039/b207595d
55. Tate MP, Urade VN, Kowalski JD et al. (2006) Simulation and interpretation of 2D diffraction patterns from self-assembled nanostructured films at arbitrary angles of incidence: from grazing incidence (above the critical angle) to transmission perpendicular to the substrate. J Phys Chem B 110:9882–9892. https://doi.org/10.1021/jp0566008
56. Soler-Illia GJAA, Crepaldi EL, Grosso D, Sanchez C (2004) Designed synthesis of large-pore mesoporous silica-zirconia thin films with high mixing degree and tunable cubic or 2B-hexagonal mesostructure. J Mater Chem 14:1879–1886. https://doi.org/10.1039/b316033e
57. De Groot F, Vankó G, Glatzel P (2009) The 1s X-ray absorption pre-edge structures in transition metal oxides. J Phys Condens Matter 21. https://doi.org/10.1088/0953-8984/21/10/104207
58. Yamamoto T (2008) Assignment of pre-edge peaks in K-edge x-ray absorption spectra of 3d transition metal compounds: electric dipole or quadrupole? X-Ray Spectrom 37:572–584. https://doi.org/10.1002/xrs.1103
59. Farges F, Brown GE, Navrotsky A et al. (1996) Coordination chemistry of Ti(IV) in silicate glasses and melts: II. Glasses at ambient temperature and pressure. Geochim Cosmochim Acta 60:3039–3053. https://doi.org/10.1016/0016-7037(96)00145-7
60. Farges F, Brown GE (1997) Ti-edge XANES studies of Ti coordination and disorder in oxide compounds: comparison between theory and experiment. Phys Rev B—Condens Matter Mater Phys 56:1809–1819. https://doi.org/10.1103/PhysRevB.56.1809
61. Bianconi A, Dell'Ariccia M, Gargano A, Natoli CR (1983) Bond length determination using XANES. In: Bianconi A, Incoccia L, Stipcich S (eds) EXAFS and near edge structure. Springer-Verlag, Berlin, p 57–61
62. Piancastelli MN (1999) The neverending story of shape resonances. J Electron Spectros Relat Phenom 100:167–190. https://doi.org/10.1016/s0368-2048(99)00046-8
63. Howard CJ, Sabine TM, Dickson F (1991) Structural and thermal parameters for rutile and anatase. Acta Crystallogr Sect B 47:462–468. https://doi.org/10.1107/S010876819100335X
64. Iwamoto S, Iwamoto S, Inoue M et al. (2005) XANES and XPS study of silica-modified titanias prepared by the glycothermal method. Chem Mater 17:650–655. https://doi.org/10.1021/cm040045p
65. Ondračka P, Nečas D, Carette M, et al. (2020) Unravelling local environments in mixed TiO2–SiO2 thin films by XPS and ab initio calculations. Appl Surf Sci 510. https://doi.org/10.1016/j.apsusc.2019.145056
66. Permpoon S, Berthomé G, Baroux B et al. (2006) Natural superhydrophilicity of sol-gel derived SiO_2-TiO_2 composite films. J Mater Sci 41:7650–7662. https://doi.org/10.1007/s10853-006-0858-1
67. Levelut C, Cabaret D, Benoit M et al. (2001) Multiple scattering calculations of the XANES Si K-edge in amorphous silica. J Non Cryst Solids 293–295:100–104. https://doi.org/10.1016/S0022-3093(01)00658-5
68. Sutherland DGJ, Kasrai M, Bancroft GM et al. (1993) Si L- and K-edge x-ray-absorption near-edge spectroscopy of gas-phase Si (CH3)x(OCH3)4-x: models for solid-state analogs. Phys Rev B 48:14989–15001. https://doi.org/10.1103/PhysRevB.48.14989
69. Li D, Bancroft GM, Kasrai M et al. (1994) X-ray absorption spectroscopy of silicon dioxide (SiO2) polymorphs: the structural characterization of opal. Am Miner 79:622–632
70. Chaboy J, Barranco A, Yanguas-Gil A et al. (2007) Si K -edge XANES study of SiOxCyHz amorphous polymeric materials. Phys Rev B - Condens Matter Mater Phys 75:075205. https://doi.org/10.1103/PhysRevB.75.075205
71. Ohnemus DC, Krause JW, Brzezinski MA et al. (2018) The chemical form of silicon in marine Synechococcus. Mar Chem 206:44–51. https://doi.org/10.1016/j.marchem.2018.08.004
72. Crepaldi EL, Soler-Illia GJAA, Grosso D et al. (2003) Controlled formation of highly organized mesoporous titania thin films: from mesostructured hybrids to mesoporous nanoanatase TiO_2. J Am Chem Soc 125:9770–9786. https://doi.org/10.1021/ja030070g
73. Tang Q, Angelomé PC, Soler-Illia GJAA, Müller M (2017) Formation of ordered mesostructured TiO2 thin films: a soft coarse-grained simulation study. Phys Chem Chem Phys 19:28249–28262. https://doi.org/10.1039/c7cp05304e
74. Jolivet J-P (2000) Metal oxide chemistry and synthesis: from solution to solid state. J. Wiley and Sons, Chichester
75. George I, Viel P, Bureau C et al. (1996) Study of the silicon/γ-APS/pyralin assembly interfaces by X-ray photoelectron spectroscopy. Surf Interface Anal 24:774–780. https://doi.org/10.1002/(SICI)1096-9918(199610)24:11<774::AID-SIA180>3.0.CO;2-X